Solid State Phenomena
ISSN: 1662-9779, Vol. 300, pp 25-46
doi:10.4028/www.scientific.net/SSP.300.25

Submitted: 2018-12-27
Revised: 2019-08-06
Accepted: 2019-08-08
Online: 2020-02-12

CHAPTER 2

Mechanical Behaviour of Thermal Oxide Scales on Stainless Steels

Valérie Parry[1,a*], Somrerk Chandra-ambhorn[2,b], Thanasak Nilsonthi[2,c] and Muriel Braccini[1,d]

[1]Université Grenoble Alpes, CNRS, Grenoble INP, SIMaP, F-38000 Grenoble, France

[2]High Temperature Corrosion Research Centre, Department of Materials and Production Technology Engineering, Faculty of Engineering, King Mongkut's University of Technology North Bangkok, 1518, Pracharat 1 Road, Bangsue, Bangkok, 10800, Thailand

[a]valerie.parry@grenoble-inp.fr, [b]somrerk.c@eng.kmutnb.ac.th, [c]thanasak.n@eng.kmutnb.ac.th, [d]muriel.braccini@grenoble-inp.fr

Keywords: stress, strain, plane stress analysis, mechanical failure, interface, adhesion energy, mode-mixity, tensile testing, inverted blister test, modified 4-point bending test

Abstract. The mechanical behaviour and adhesion properties of thermal oxide scales are key issues for steel processing and long-term durability. This chapter aims at taking up the various aspects to be considered for such studies. The first part is devoted to a description of the origin of stress and stress quantification. Then, description of mechanical failure and damaging patterns of thermal oxide scales will be given. Finally, definitions of adhesion energy as well as quantitative methods to measure adhesion energy will be proposed. An appendix describing the hypotheses and the constitutive equations for plane stress analysis, which suits to oxide scales, is also given The purpose is enriched by references in particular to Alain Galerie's co-workers' publications.

2.1 Development and Quantification of Stress

The durability at high temperature of stainless steels depends on the resistance of the protective chromia-rich scale to chemical and/or mechanical failure. The tricky point is the coupling between the mechanical behaviour of the metal-oxide system and its chemical and microstructural changes during the oxide growth. Mechanical stress accumulation in oxide layer and metallic substrate is the driving force for the mechanical failure. Whereas resistance to high-temperature oxidation assumes the growth and the maintenance of a protective oxide scale which separates the metal from its environment, steel processing requires several de-scaling operations. Since it is desirable to be able to predict oxide scale adhesion, stress generation and relief in oxide scales are of importance. Although stresses can result from an external loading applied during high temperature treatment, additional stresses are generated during the oxidation process: growth stresses and thermal stresses. For this section, readers are also invited to consult Refs. [1–4].

2.1.1 Growth Stresses

Growth stresses happen during the isothermal part of the oxidation process. It can result from volume difference or epitaxial relationship between the metal and the oxide or from compositional changes or gradient in point defects.

The specific volume of the oxide is different from that of the metal which is consumed. Oxidation causes volume changes which are adjusted by strain in the oxide. In the case of scale formation occurring by inward diffusion of oxygen, the molar volume ratio described by Pilling and Bedworth (Pilling-Bedworth Ratio, PBR), may be first used to indicate the type of growth stress.

$$\mathrm{PBR} = \frac{\Omega_{\mathrm{M_aO_b}}}{\mathrm{a} \cdot \Omega_{\mathrm{M}}} \tag{2.1}$$

where $\Omega_{M_aO_b}$ is the molar volume of the metal oxide M_aO_b and Ω_M is the molar volume of the metal M.

If the ratio is greater than one, the resulting expansion could put the oxide into compression. In the case of a ratio lower than one, the oxide scale is subjected to tensile stress and a discontinuous oxide could result. Examples of molar volume ratios are displayed in Table 2.1.

Table 2.1 Pilling-Bedworth Ratio (PBR) of some common metal/oxide couples [2, 5].

Oxide/metal	Al_2O_3/Al	ZrO_2/Zr	Cu_2O/Cu	NiO/Ni	FeO/α-Fe	TiO_2/Ti
PBR	1.28	1.56	1.64	1.65	1.68	1.73
Oxide/metal	SiO_2/Si	Cr_2O_3/Cr	Fe_3O_4/α-Fe	Fe_2O_3/α-Fe	Ta_2O_5/Ta	Nb_2O_5/Nb
PBR	1.9	2.07	2.10	2.14	2.5	2.68

The volume change linked to new oxide formation has to be accommodated at the metal/oxide interface. Considering no stress relieving mechanism, the resulting strain in the oxide ε_{ox} is

$$\varepsilon_{ox} = (\mathrm{PBR})^{1/3} - 1 \tag{2.2}$$

Considering an elastic behaviour for the oxide, the biaxial stress state (see Appendix) in the oxide would be

$$\sigma_{ox} = -\frac{E_{ox}}{1-\nu_{ox}}\varepsilon_{ox} \tag{2.3}$$

where E_{ox} is the elastic modulus and ν_{ox} is Poisson's ratio of the oxide.

Although the PBR description is qualitatively useful, its quantitative use is limited. First, it does not apply to oxide growth by outward diffusion where oxide formation takes place at the outer free surface. In this case, oxide is not constrained to occupy the volume of the consumed metal and the stress in the scale is relatively low. In the case of oxide growth by inward anionic diffusion, the stress level calculated from Eq. 2.3 is overestimated. This approach assumes that no additional stress relaxation mechanisms such as plastic deformation (creep, dislocation motion) or fracture, take place. Moreover, complex transport phenomena such as mixed transport, grain boundary diffusion are not taken into account.

At the early stages of the oxide growth, the first germs to form are considered to have an epitaxial relationship with the metal. This lattice parameter mismatch between the metal and the oxide results in stress development.

The selective oxidation results in the depletion of one or more elements in the underneath metal substrate and thus the change in the alloy lattice parameter. In the same manner, dissolution of oxygen into metal with high solubility, volume change associated with internal precipitation of oxide or oxidation of internal carbides can cause volume expansion and produce stresses.

Variation of lattice parameter across the scale due to a gradient in point defects can generate stresses in oxide allowing deviations from stoichiometry. Oxide growth by outward metal diffusion results in vacancy injection in the substrate. Relaxation around the vacancies induces a lattice-parameter variation resulting in stresses in the substrate or stress relief by enhancing creep within the metal.

2.1.2 Thermoelastic Stress

Since metals and oxides have different thermal expansion coefficients (α), thermoelastic stress can be generated during temperature change. α is generally defined as

$$\alpha = \frac{1}{L}\frac{\mathrm{d}L}{\mathrm{d}T} \tag{2.4}$$

where L is the length of the considered material and $\mathrm{d}L/\mathrm{d}T$ is the change of length with respect to the temperature T.

Examples of thermal expansion coefficients are displayed in Table 2.2.

Table 2.2 Thermal expansion coefficients of metals and oxides [3, 6].

System	Metal coefficient ($\times 10^{-6}$ K^{-1})	Oxide coefficient ($\times 10^{-6}$ K^{-1})	Ratio	Temperature range (ºC)
Fe/FeO	15.3	12.2	1.25	100–900
Fe/Fe_2O_3	15.3	14.9	1.03	20–900
Ni/NiO	17.6	17.1	1.03	20–1000
Co/CoO	14.0	15.0	0.93	25–350
Cr/Cr_2O_3	9.5	7.3	1.30	100–1000
Cu/Cu_2O	18.6	4.3	4.32	20–750
Cu/CuO	18.6	9.3	2.00	20–600

An intact and adherent oxide scale is considered. This implies that any deformation of the metallic substrate is transferred to the scale. Considering an elastic behaviour for both metal and oxide and a homogeneous stress, the resulting strain in the oxide $\mathrm{d}\varepsilon_{\mathrm{ox}}$ is

$$\mathrm{d}\varepsilon_{\mathrm{ox}} = \alpha_{\mathrm{ox}}\mathrm{d}T + \left(\frac{1-\nu_{\mathrm{ox}}}{E_{\mathrm{ox}}}\right)\mathrm{d}\sigma_{\mathrm{x}} \tag{2.5}$$

The biaxial stress state in the oxide is

$$\mathrm{d}\sigma_{\mathrm{ox}} = -\frac{E_{\mathrm{ox}}(\alpha_{\mathrm{ox}}-\alpha_{\mathrm{m}})\mathrm{d}T}{\frac{E_{\mathrm{ox}}h_{\mathrm{ox}}}{E_{\mathrm{m}}h_{\mathrm{m}}}(1-\nu_{\mathrm{m}})+(1-\nu_{\mathrm{ox}})} \tag{2.6}$$

where h_{ox} and h_{m} are the thicknesses of scale and metallic substrate respectively, E_{ox} is the elastic modulus of the oxide, ν_{ox} and ν_{m} are Poisson's ratios of the oxide and metal respectively.

For a thin oxide scale on thick metallic substrate, the biaxial stress state in the oxide can be approximated by

$$\mathrm{d}\sigma_{\mathrm{ox}} = -\frac{E_{\mathrm{ox}}(\alpha_{\mathrm{ox}}-\alpha_{\mathrm{m}})\mathrm{d}T}{(1-\nu_{\mathrm{ox}})} \tag{2.7}$$

The thermally induced stress depends on the magnitude of temperature change and the difference between the thermal expansion coefficient of the oxide and the metal. According to Table 2.2, the coefficients of thermal expansion of metals are typically higher than that of oxides. It means that during cooling, the oxide scale will be subjected to compressive stress. It should be noted that this approach assumes that no stress relaxation mechanisms are in effect.

2.1.3 Quantification of Stress

The stress level in the oxide cannot be measured directly. Its determination requires assumptions. X-Ray diffraction or Raman spectroscopy are based on the measurements of strain of the oxide lattice [7–10]. Fig. 2.1 displays the evolution of compressive stress in the oxide scale thermally grown on stainless steels, deduced from the Cr_2O_3 Raman peak shift [10]. Deflection technique is sensitive and permits to obtain a stress distribution. However creep data for both oxide and metal phases are needed. For more details readers are invited to consult Ref. [11].

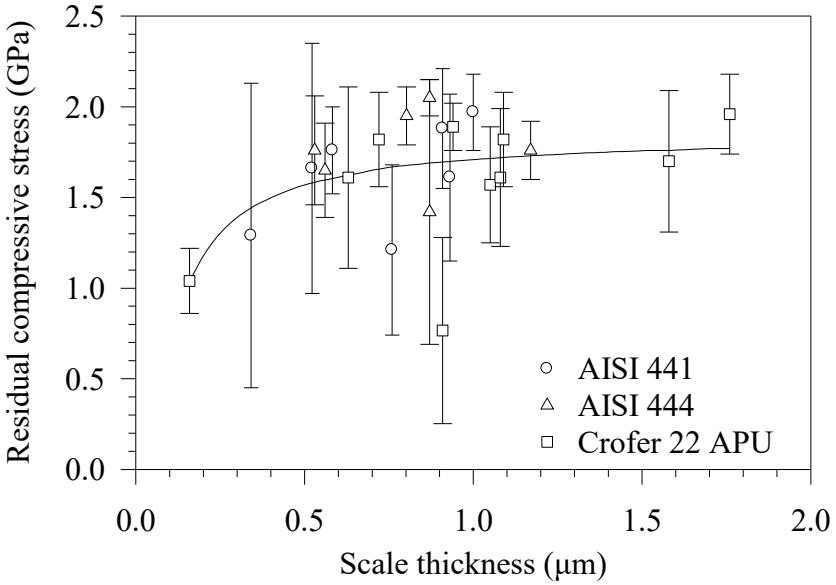

Fig. 2.1. Evolution of residual compressive stress, deduced from Cr_2O_3 Raman peak shift, according to the thickness of oxide scale thermally grown on ferritic stainless steels. Redrawn and adapted from S. Chandra-ambhorn et al., J. Power Sources 171 (2007) 688–695 [10].

2.2 Mechanical Failure

Stresses generated by oxide growth and thermal mismatch can be accommodated by elastic or plastic deformation of the oxide and/or of the metal. However, when the stored energy in the oxide scale exceeds the fracture resistance of the oxide or of the metal/oxide interface, mechanical failure happens. Fracture is the most effective relaxation mode but it has severe consequence. Since fresh metal is exposed to oxidising environment, the corrosion rate increases.

2.2.1 Damaging Patterns and Fracture Opening Modes

Damaging patterns depends on the stress state, the properties and the microstructure of both oxide and metal. It varies from micro-cracks to spallation. If the oxide scale is put into tension, the appearance of cracks happens as soon as oxide yield stress value is reached. This limit corresponds to less than 1% of deformation, even at high temperature. If the oxide scale is under compressive stresses, which is the most common case, the scale will fracture and spall.

Two conditions are necessary for spallation: transverse cracking and interface decohesion. Decohesion can happen at the metal/oxide interface (adhesive failure) or along oxide scale layer interfaces (cohesive failure). Two cracking and spallation routes caused by compressive stress in the oxide, illustrated in Fig. 2.2, can be considered.

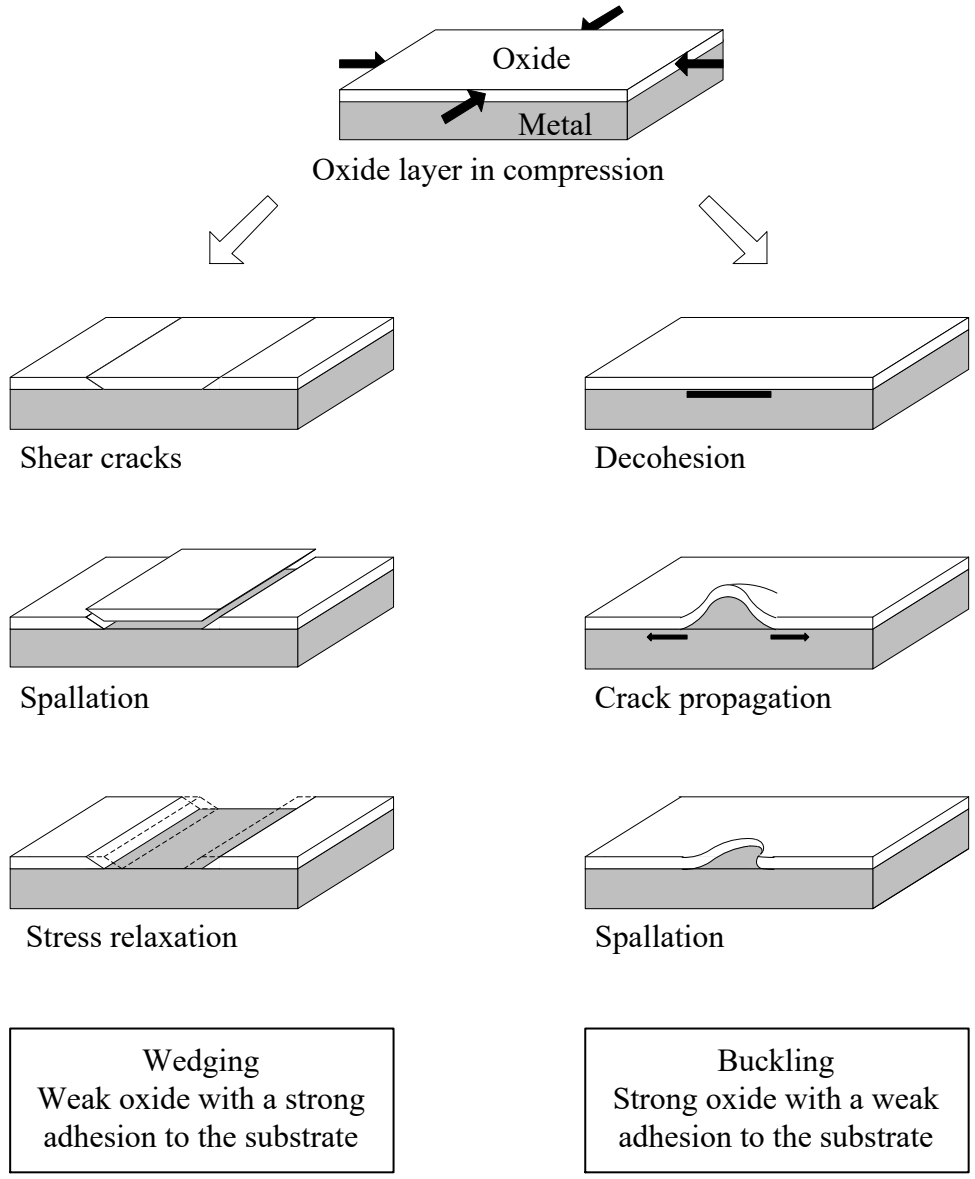

Fig. 2.2. Spallation routes of oxide scale under compressive stress depending on the relative fracture resistance of the oxide and of the metal/oxide interface. Adapted from H.E. Evans, Inter. Mater. Rev. 40 (1995) 1–40 [4].

The first, called wedging, is characteristic of mechanically weak oxides with a strong adhesion to the substrate. It supposes primarily the failure of the oxide scale by compressive shear crack due, for example, to temperature drop or mechanical loading. The origin of oxide scale failure is linked to defects present in the scale.

The second, called buckling, describes the behaviour of a strong oxide with a weak interface with the substrate. Spallation starts from the buckling of the oxide scale, i.e. the metal/oxide interface decohesion. The origin of buckling may be linked to voids accumulation or segregation of elements at the metal/oxide interface.

In the case of a thin oxide of thickness h under biaxial compressive stress (see Appendix), the critical stress σ_c necessary to form a buckle of radius a is

$$\sigma_c = 1.22 \frac{E}{(1-\nu^2)} \left(\frac{h}{a}\right)^2 \tag{2.8}$$

Since σ_c increases with the square of the scale thickness, buckling route is less likely for thick oxide.

Depending on the mechanical stress experienced by a crack, three linearly independent fracture opening modes can occur: mode I, or mode of normal opening of the crack, and modes II and III, opening modes in shear as shown in the Fig. 2.3.

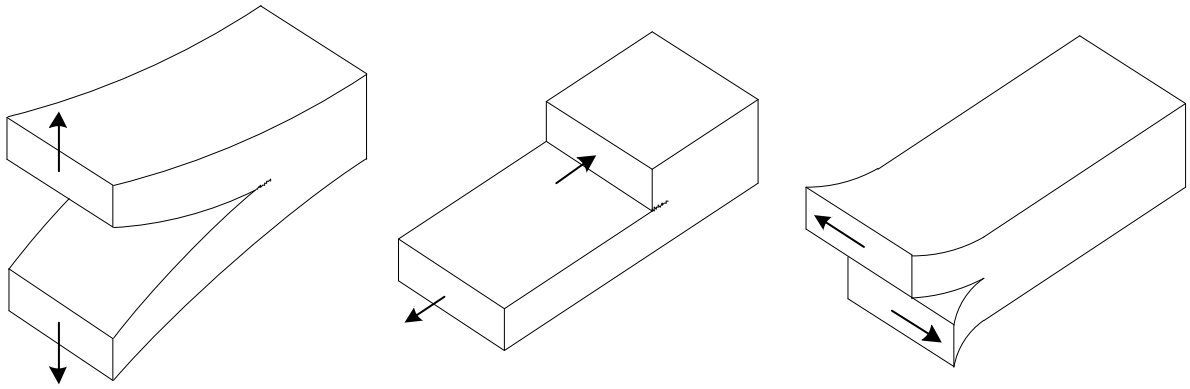

Fig. 2.3. The three fracture modes.

In a homogeneous isotropic material, the propagation of a crack is usually done such that the stress field at the crack tip is purely tensile (mode I). However, in the case of an interfacial crack, the propagation is generally done in mixed mode (mode I and mode II combined). This mode-mixity can be defined by an angle ψ expressing the ratio between shear (τ) and normal (σ) stresses as follows:

$$\psi = \tan^{-1}\left(\frac{\tau}{\sigma}\right) \tag{2.9}$$

2.2.2 Criteria to Quantify the Adhesion Energy

Adhesion of oxide scales on metals can be assessed by qualitative consideration on the metal/oxide interface or by direct measurement of spallation in service. Adhesion and thus fracture are key parameters to better understand spallation phenomena. Two main interrelated conditions for fracture are generally proposed: energy or stress intensity factor approaches.

The energy criterion for fracture arises from Griffith's work [12] in which the presence of a pre-existing crack is considered (Fig. 2.4). The energy stored in the volume (E_{tot}) is the sum of the potential energy (E_{pot}) arising from the stored elastic energy (E_{el}) and the work performed by external forces (W_{ext}) and of the surface energy (E_{surf}):

$$E_{pot} = E_{el} - W_{ext} \tag{2.10}$$

$$E_{surf} = 2\gamma A \tag{2.11}$$

where γ is the interfacial energy and A is the crack area.

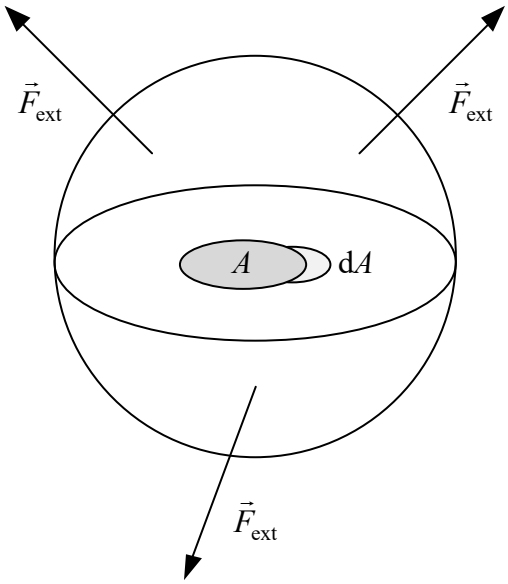

Fig. 2.4. Crack of surface A in a volume submitted to external forces.

The energy releases by the crack growth is the energy release rate *G*. The energy balance requires a net decrease in energy and *G* is defined as

$$G = -\frac{\partial E_{tot}}{\partial A} \tag{2.12}$$

According to Griffith, fracture occurs when the energy release rate is sufficient to supply the energy requirements for the creation of new fracture surfaces.

$$\frac{\partial E_{tot}}{\partial A} + 2\gamma = 0 \tag{2.13}$$

This approach yields a measure of G_c, the fracture energy, or toughness, of the interface, which is

$$G_c = 2\gamma \tag{2.14}$$

G_c is the energy value required to extend a crack over unit area. When the stored elastic energy in the oxide scale exceeds the fracture resistance of the interface, crack propagation and spallation will occur.

The value of G_c cannot be directly equated to that needed solely to rupture molecular bonds. So G_c differs from the thermodynamic adhesion energy W_{ad} derived from the metal, oxide and interfacial surface energies:

$$W_{ad} = \gamma_m + \gamma_{ox} - \gamma_i \tag{2.15}$$

G_c is several orders of magnitude higher than W_{ad}, since it encompasses the dissipative-energy losses occurring around the crack tip (W_{dis}), that is, viscoelastic and plastic energy losses in the crack tip damage zone. In many cases W_{ad} lies in the order of 1 J m^{-2} while G_c is between 1 and 1000 J m^{-2}.

Moreover, G_c value depends on the propagation mode of the crack (i.e. the mode-mixity). According to Fig. 2.5, the lowest values of G_c are obtained for the lowest value of ψ and corresponds to a fracture opening normal to the plane of the crack (mode I). Increasing mode II contribution increases G_c values.

Phenomenological laws have been designed to describe this dependence, for example the one proposed by Hutchinson and Suo [13] which includes a parameter η rendering the dependency of the fracture energy to mode-mixity in the following form:

$$G_c(\psi) = G_{Ic}(1 + \tan^2(\eta\psi)) \tag{2.16}$$

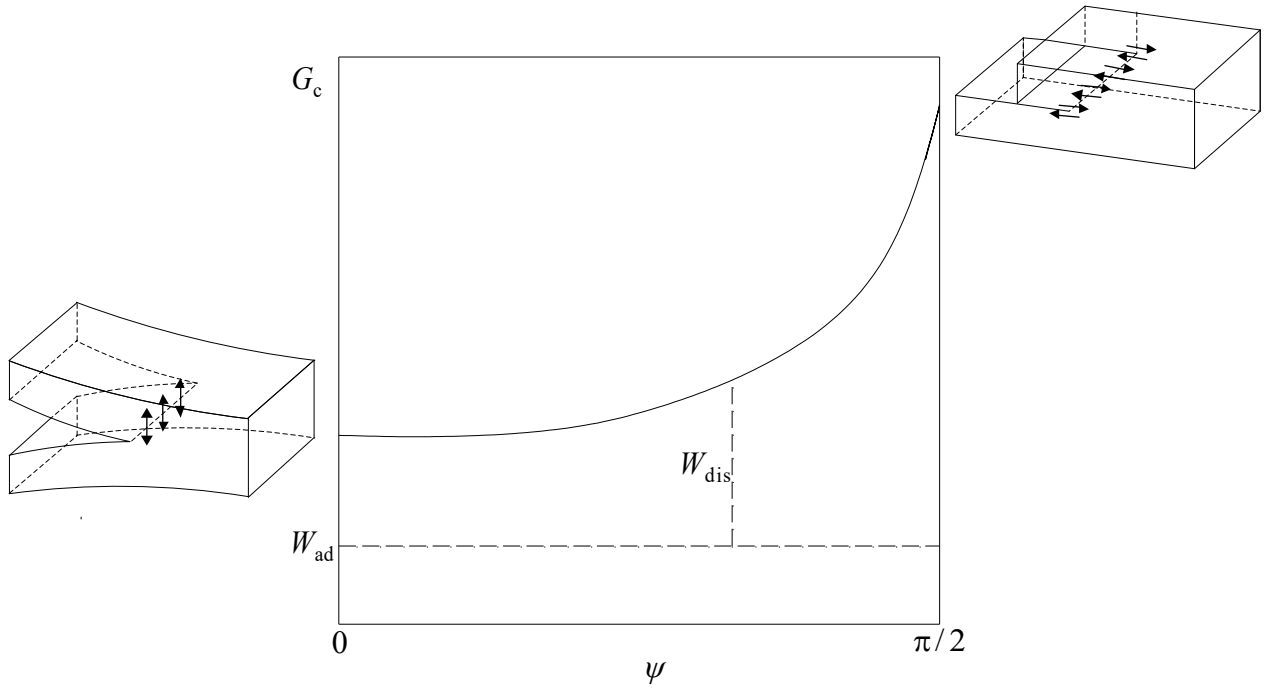

Fig. 2.5. Evolution of G_c according the mode-mixity angle ψ. Redrawn and adapted from M. Braccini, Chapter 4 Interface adherence, in: M. Braccini, M. Dupeux (Eds.), Mechanics of Solid Interfaces, John Wiley & Sons, USA, 2012 [14].

The stress-intensity factor approach of fracture energy is related to Irwin [15]. According to his work, the stress field around a sharp crack in a linear-elastic material can be defined by a single parameter, the stress-intensity factor K. Fracture occurs when the value of K exceeds some critical value K_c. Thus, K is a stress-field parameter independent of the material, whereas K_c often referred to as the fracture toughness, is a measure of a material property.

Griffith and Irwin approaches are linked. The energy criterion clears the defect size and shape whereas values of K_I depend on crack features. In the case of an infinite plane with a crack perpendicular to the loading direction (propagating in mode I) submitted to an uniaxial tensile stress σ, the relationship between energy release rate and stress intensity factor in mode I is

$$G = K_I^2 \cdot \frac{1}{E} \tag{2.17}$$

where E is the elastic modulus and σ is the stress field.

Eqs. 2.18 and 2.19 are two examples of stress intensity factors in infinite volumes. The case of a straight crack of length 2*a* and of a circular crack of radius *a* perpendicular to the loading direction (mode I) are illustrated Fig. 2.6.

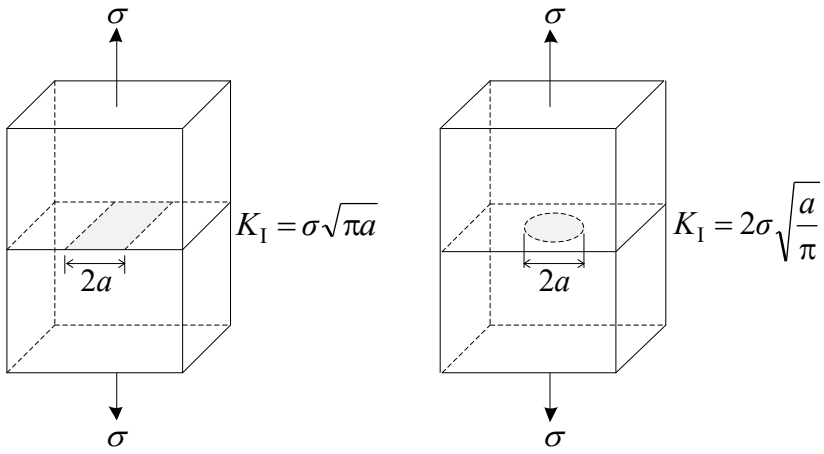

Fig. 2.6. Examples of stress-intensity factors for a straight crack of length 2*a* (left) and a circular crack of radius *a* (right) perpendicular to the loading direction (mode I) in infinite volumes. Redrawn and adapted from T.L. Anderson, Fracture Mechanics: Fundamental and Applications, third ed., CRC Press, USA, 2005 [16].

$$K_I = \sigma\sqrt{\pi a} \qquad \text{for a straight crack of length } 2a \tag{2.18}$$

$$K_I = 2\sigma\sqrt{\frac{a}{\pi}} \qquad \text{for a circular crack of radius } a \tag{2.19}$$

2.3 Experimental Determination of Adhesion Energy

To assess the scale adhesion, several experiments have been designed to determine quantitative values of adhesion energy of metal-oxide system. Each configuration is characterised by loading conditions which act on the crack propagation. Indeed, in the case of a metal/oxide interface the difference between the mechanical behaviour of the two materials of both sides of the interface generates asymmetry even if the geometry and the loading are symmetrical. As long as the interface represents the easiest break path, the crack is trapped and will not bifurcate easily as it would in a homogeneous fragile material. Thus mixed-mode conditions of loading affect the propagation of the interfacial crack and thus the value of adhesion energy. As a consequence, comparison between values of adhesions energy obtained from different tests must be done cautiously.

In the following, three methods will be described: the inverted blister test, the modified 4-point bending test and *in-situ* tensile testing. The angle ψ expressing the ratio between shear (mode II) and normal (mode I) stresses has been evaluated for the three tests [17]. Results are presented in Table 2.3. The loading of the inverted blister testing is mainly in mode I, whereas tensile testing loading is mainly in mode II. The modified 4-points bending test corresponds to equivalent contributions of mode I and mode II.

Table 2.3 Mixed mode angles for different method of adhesion energy measurements [17].

Test	Inverted blister test	Modified 4-points bending test	Tensile testing
ψ angle (°)	25	40	close to 90

For a given test, the reproducibility and the energy released during crack initiation and crack propagation are different. Crack initiation is a stochastic mechanism which may require a high value of energy to happen whereas crack propagation is more reproducible. Thus it provides a better description of the adhesion properties of an interface. Adhesion test measurements have to be performed during crack propagation although it is not always possible.

The *inverted blister test* is a configuration of the blister test [18] adapted to the brittle nature of the oxide [19–20]. One side of an oxidised metallic foil is glued, on the oxide side, over the central hole of a sample holder as sketched in Fig. 2.7 (top). The relative thicknesses of the different layers are not scaled in the figure. The thickness of the stainless steel foil is around 150 μm while the thermal oxide is about 1–3 μm thick, see for examples Ref. [21]. Different glues can be used depending on the toughness of the metal/oxide interface. For example, Araldite® allows measuring adhesion energies up to ~200 J m^{-2}. The oxide layer is locally removed by grinding through the sample holder hole in order to reveal the bare metal. The test, described on Fig. 2.7 (middle and bottom), consists in injecting in the hole an inert and incompressible fluid at a controlled pressure with a micro-syringe to create a blister. The altitude and the diameter of the blister can be measured by projecting interference fringes on the bulge surface, giving iso-altitude lines by contour analysis profilometry. The evolution of the fluid pressure (P) as a function of the bulge attitude (h) is shown in Fig. 2.8.

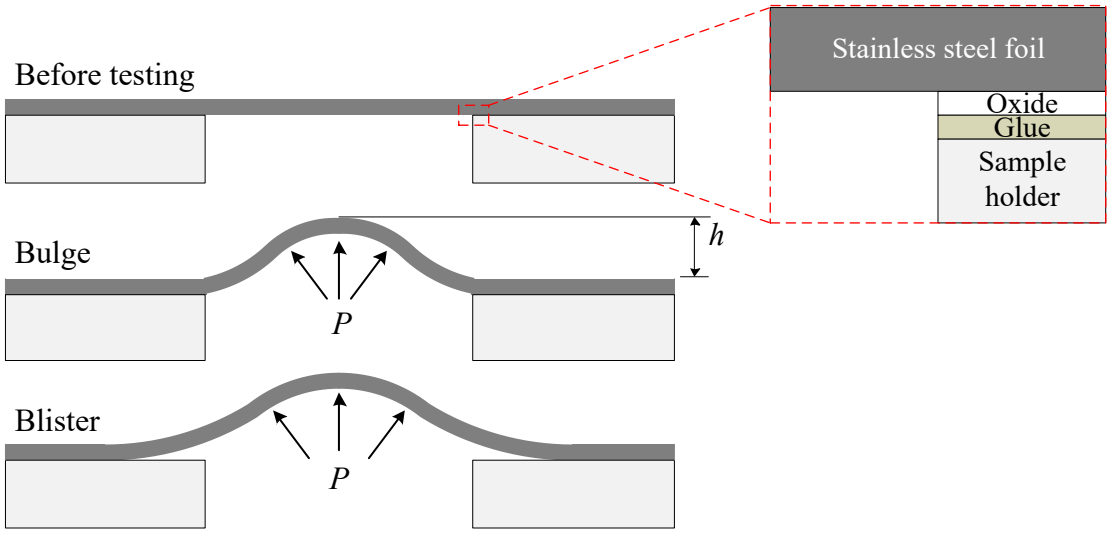

Fig. 2.7. Schematics of the experimental set-up (top) and the two stages of the inverted blister test (middle and bottom). Adapted from J. Mougin et al., Mater. Sci. Eng., A 359 (2003) 44–51 [21] and from R.J. Hohlfelder et al., Mat. Res. Soc. Symp. Proc. 356 (1995) 585–590 [22].

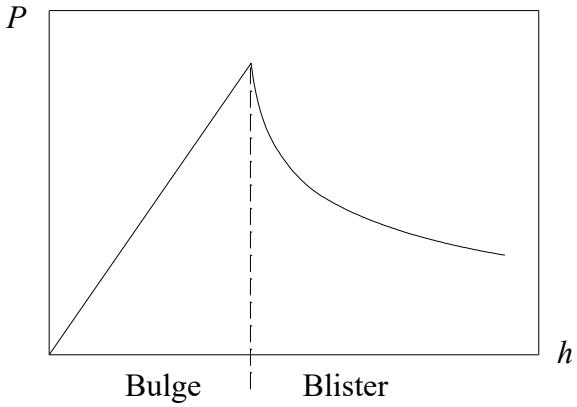

Fig. 2.8. Evolution of the fluid pressure according to the bulge altitude. Redrawn and adapted from M. Braccini, Chapter 4 Interface adherence, in: M. Braccini, M. Dupeux (Eds.), Mechanics of Solid Interfaces, John Wiley & Sons, USA, 2012 [14].

When increasing the amount of injected fluid, the metallic part of the sample blow up, forming a bulge of constant diameter. The bulge altitude increases with the fluid pressure. This "bulge state" allows measuring the Young's modulus and the residual stress of the metallic foil. For a critical pressure, damaging happens and a circular crack propagates along the metal/oxide interface. The diameter of the bulge increases with the amount of injected fluid. The bulge altitude increases as well whereas the fluid pressure decreases. It is assumed that no energy release occurs in the oxide layer during the crack propagation along the metal/oxide interface, in particular the long-range average biaxial stress in the oxide layer (see Appendix) do not contribute to crack propagation. Only the energy afforded by the injected fluid is taken into account. So, the pressure drop curve of the "blister stage" is described by an energy balance between the energy supplied to the system by the fluid under pressure and the energy consumed by the deformation of the metallic foil and by the propagation of the interfacial crack. In the case of an elastic behaviour of the metallic substrate, the pressure drop is described by a hyperbole [21, 22].

$$G_c = CPh \tag{2.20}$$

where P is the fluid pressure, h is the bulge altitude and C is a constant depending on the mechanical properties and the residual stress of the metallic foil.

Refs. [17, 21, 23, 24] from Alain Galerie's co-workers, provide applications of the inverted blister test for adhesion energy measurements.

The geometry of the *modified 4-point bending test* is presented in Fig. 2.9 [25–27]. The proportions between the different layers in Fig. 2.9 are not scaled. Stiffeners or counterplates are glued on the oxide scale. The notch in the counterplates corresponds to a pre-crack. The system is submitted to a vertical loading at a constant rate, leading first to elastic bending of the sample, then to interface decohesion and crack propagation. The force F_p corresponding to crack propagation is constant. The typical evolution of the applied force (F) as a function of the displacement (Δl) during the test is shown in Fig. 2.10. In the case of identical thicknesses and mechanical properties of the substrate and of the counterplates, the adhesion energy is derived from F_p as follows:

$$G_c = \frac{21}{16}\frac{F_p^2 l^2}{\overline{E} h^3 b^2} \tag{2.21}$$

Here $h = h_1 + h_2$ and $\overline{E}$ equals E or $E/(1-\nu^2)$ for the plane stress and plane strain assumption respectively. E and ν are respectively the elastic modulus and the Poisson's ratio of the substrate which is equal to the counterplate under this assumption [14]. Illustrations of adhesion energy measurements with 3- and 4-point bending tests can be found in Refs. [17, 27].

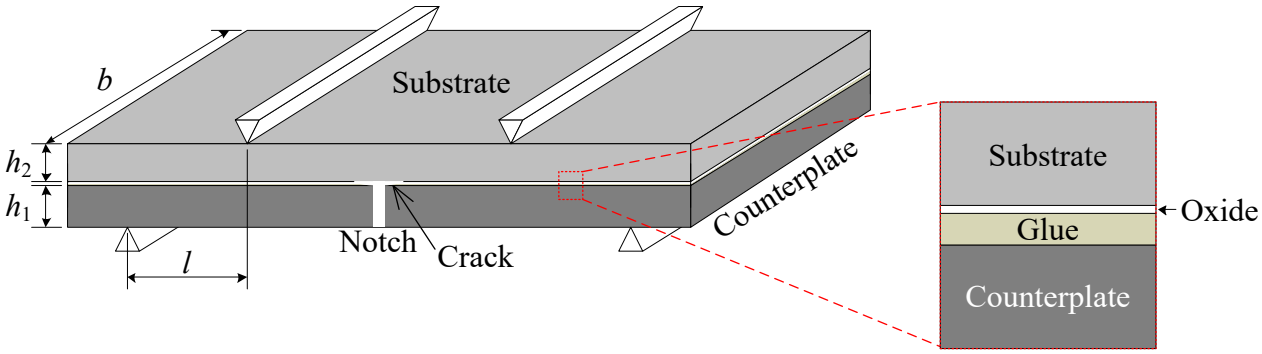

Fig. 2.9. Schematic of the 4-point bending test and typical force displacement curve. Adapted from P.G. Charalambides et al., Mech. Mater. 8 (1990) 269–283 [25], I. Hofinger et al., Int. J. Fract. 92 (1998) 213–220 [26] and M. Zhe et al., J. Adhes. Sci. Technol. 26 (20120 1-17 [27].

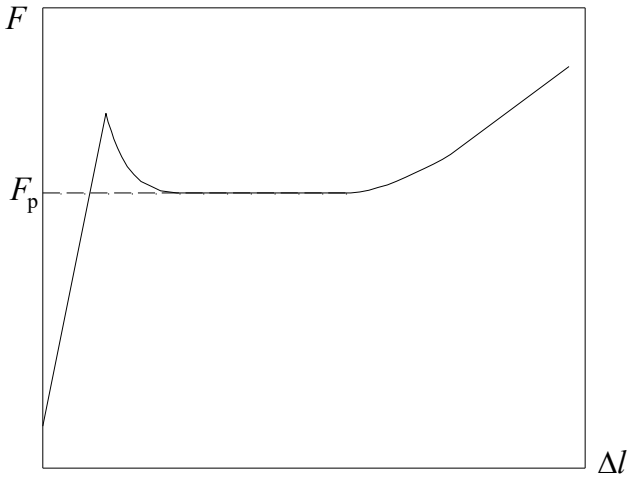

Fig. 2.10. Typical force-displacement curve during the 4-point bending test. Adapted from M. Zhe et al., J. Adhes. Sci. Technol. 26 (2012) 1–17 [27].

For the *tensile testing*, oxidised specimens are loaded in a tensile machine designed to be placed under an optical microscope or in the scanning electron microscope chamber. The central region of the specimen is observed whereas a regular elongation rate is applied. The displacement motion is interrupted in order to acquire images of the sample surface. Sequential micrographs of the evolution of the damage in the oxide scale are collected according to the applied strain [9, 10, 17, 24, 28–38].

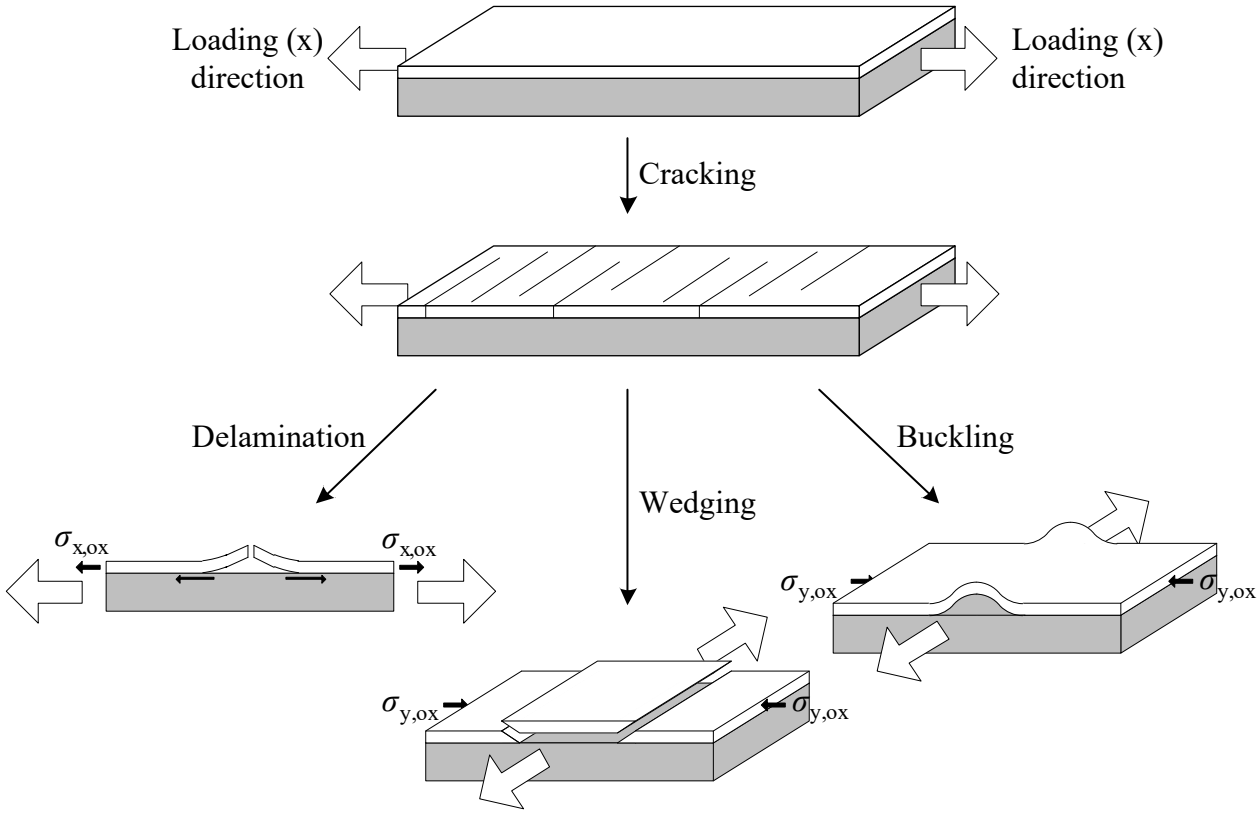

Fig. 2.11. The possible scenarios for scale decohesion during tensile testing. $\sigma_{x,ox}$ and $\sigma_{y,ox}$ are normal stresses exerted on the oxide film in the loading direction and in the direction perpendicular to the loading direction respectively.

At the beginning of the test, the substrate and the oxide scale are elastically strained. Whereas the plastic deformation of the substrate occurs, cracks happen in the oxide scale. These cracks allow a stresses redistribution, in particular shear stresses appearance at the metal/oxide interface. The volume conservation in plasticity imposes a compressive strain of the scale in the direction perpendicular to the traction direction. Depending on the scale adhesion, different scenarios for decohesion, displayed in Fig. 2.11, are possible: delamination, wedging (cracking of the layer then detachment) and buckling (detachment then buckling).

The evolution of the spallation ratio as a function of the imposed strain for thermal oxide scales grown on AISI 444 at 800 ºC in synthetic air for different oxidation times, giving different scale thicknesses, are displayed in Fig. 2.12. The spallation ratio is measured from electronic or optical images and corresponds to the spalled area normalised by the total area of the sample (metal and oxide) in the image. According to Fig. 2.12, the beginning of spallation as well as the saturation of the spallation ratio of the thickest oxide happen for the lowest imposed strain value. Thus, the related curves of the spallation ratio with respect to the imposed strain are characterised by high slope which indicates the higher sensibility of thick oxides to be spalled out with the increase of the imposed strain. This behaviour was observed by François Toscan [29] and many times later in the studies under Galerie's supervision [10, 30]. It is therefore called the "François effect" as named by A. Galerie. The determination of adhesion energy from tensile testing experiments at the strain initiating the first spallation is described in the following part.

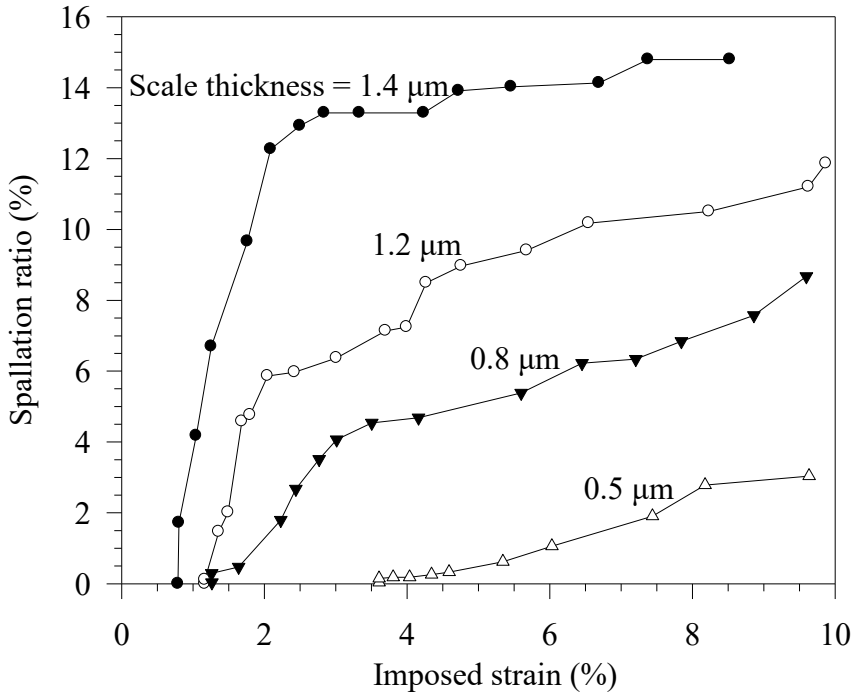

Fig. 2.12. Spallation ratio as a function of the imposed strain of AISI 444 oxidised at 800 ºC in synthetic air to obtain different oxide thicknesses. Redrawn and adapted from S. Chandra-ambhorn et al., J. Power Sources 171 (2007) 688–695 [10].

2.4 Galerie-Dupeux Model for the Calculation of Adhesion Energy from Tensile Testing

Adhesion energy can be determined from tensile testing. This approach relies on the calculation of the energy stored in the oxide until spallation takes place.

Oxides scales thermally grown on thick substrate can be considered as thin flat plates with an homogeneous microstructure that are acted upon only by load forces that are parallel to them. The scales are under plane stress state in the plane of the oxide (x, y), the stress vector along the direction z perpendicular to the oxide film is zero.

Considering an elastic behaviour of the oxide scale, the strain energy is

$$w = \sum_{i,j} \frac{1}{2} \sigma_{ij} \varepsilon_{ij} \tag{2.22}$$

M. Dupeux and A. Galerie proposed that the evolution of the stress in the oxide during tensile testing can be described as a succession of 3 stages [9, 10, 17, 24, 29–37]. This approach considers an elastic-plastic behaviour of the metallic substrate.

Stage I describes the residual compressive stress state of the oxide before tensile testing. The residual elastic strain energy in the oxide is related to growth and thermal stresses occurring during oxidation and cooling down respectively. These stresses put the oxide scale into compression. The equibiaxial stress state in the plane of the oxide (x, y) is

$$\sigma_{xx} = \sigma_{yy} \tag{2.23}$$

$$\sigma_{ij} = 0 \text{ for } i \neq j \tag{2.24}$$

$$\sigma_{zz} = 0 \tag{2.25}$$

The resulting strain in the oxide in the direction i where i, j stand for x or y (ε_i) is

$$\varepsilon_i = \frac{\sigma_i}{E_{ox}} - \frac{\nu_{ox}\sigma_j}{E_{ox}} = \frac{\sigma_i}{E_{ox}} - \frac{\nu_{ox}\sigma_i}{E_{ox}} = \left(\frac{1-\nu_{ox}}{E_{ox}}\right)\sigma_i = \frac{\sigma_i}{M} \tag{2.26}$$

with

$$M = \frac{E_{ox}}{1-\nu_{ox}} \tag{2.27}$$

where E_{ox} is the elastic modulus of the oxide scale and ν_{ox} is the Poisson's ratio of the oxide scale.

Finally, the residual elastic strain energy in the direction i during stage I ($w_{res,i}$) is

$$w_{res,i} = \frac{1}{2}\sigma_i \varepsilon_i = \frac{1}{2}\frac{\sigma_i^2}{M} = \frac{1}{2}\frac{\sigma_{res}^2}{M} \tag{2.28}$$

and the total residual elastic strain energy (w_{res}) is

$$w_{res} = w_{res,x} + w_{res,y} = \frac{\sigma_{res}^2}{M} \tag{2.29}$$

The residual elastic strain energy in each direction corresponds to the shaded area on the stress-strain representation displayed in Fig. 2.13.

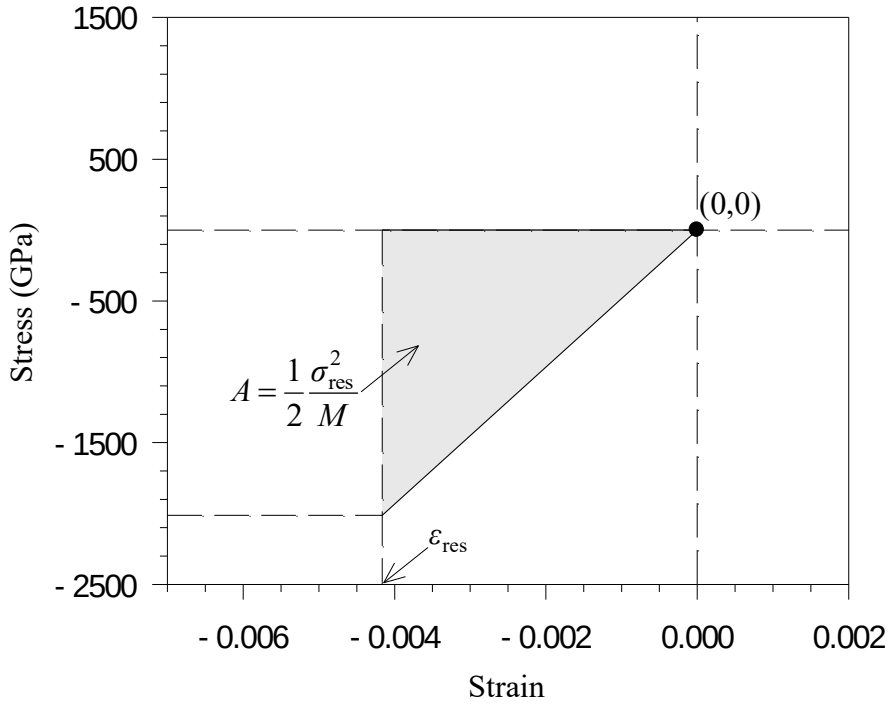

Fig. 2.13. Representation of the elastic stored energy in the oxide scale under compressive stress (stage I).

S**tage II** describes the beginning of tensile testing, until the metallic substrate reaches its yield point. Assuming an intact and adherent oxide scale, the substrate deformations are transferred to the scale:

$$\varepsilon_{x,ox} = \varepsilon_{x,m} \tag{2.30}$$

$$\varepsilon_{y,ox} = \varepsilon_{y,m} = -\nu_m \varepsilon_{x,m} \tag{2.31}$$

Here, $\varepsilon_{x,ox}$ and $\varepsilon_{x,m}$ are respectively the strain components in the tensile (x) direction in oxide and metal respectively, while $\varepsilon_{y,ox}$ and $\varepsilon_{y,m}$ are the strain components in the perpendicular (y) direction in the oxide and metal respectively.

According to Eq. 2.60 from Appendix describing the plane stress analysis, the planar stress in the oxide in the direction i where i stands for x or y ($\sigma_{i,ox}$) is

$$\sigma_{i,ox} = \frac{E_{ox}}{1-\nu_{ox}^2}(\varepsilon_{i,ox} + \nu_{ox}\varepsilon_{j,ox}) \tag{2.32}$$

According to Eq. 2.32 the stresses in the oxide can be written as a function of $\varepsilon_{x,m}$ as follows:

$$\sigma_{x,ox} = \frac{E_{ox}}{1-\nu_{ox}^2}(1-\nu_{ox}\nu_m)\varepsilon_{x,m} \tag{2.33}$$

$$\sigma_{y,ox} = \frac{E_{ox}}{1-\nu_{ox}^2}(\nu_{ox}-\nu_m)\varepsilon_{x,m} \tag{2.34}$$

The components of the elastic strain energy due to tensile testing during Stage II (w_{el}) in oxide in both *x* and *y* directions are

$$w_{\mathrm{el}_{\mathrm{x,ox}}} = \frac{1}{2}\left(\frac{E_{\mathrm{ox}}}{1-v_{\mathrm{ox}}^2}\right)(1-v_{\mathrm{ox}}v_{\mathrm{m}})\varepsilon_{\mathrm{x,m}}^2 \tag{2.35}$$

$$w_{\mathrm{el}_{\mathrm{y,ox}}} = \frac{1}{2}\left(\frac{E_{\mathrm{ox}}}{1-v_{\mathrm{ox}}^2}\right)(v_{\mathrm{m}}^2-v_{\mathrm{ox}}v_{\mathrm{m}})\varepsilon_{\mathrm{x,m}}^2 \tag{2.36}$$

In the particular case of the same Poisson's ratios for metal and oxide, the stress along *y* axis is zero and there is no elastic stored energy in this direction. The elastic strain energy is simplified as follows:

$$w_{\mathrm{el,ox}} = \frac{1}{2}E_{\mathrm{ox}}\varepsilon_{\mathrm{x,m}}^2 \tag{2.37}$$

Stage III corresponds to the phase for which plastic deformation of the substrate occurs without oxide scale spallation, the oxide is still intact and adherent and so the plastic deformations of the substrate are transferred to the scale.

$$\varepsilon_{\mathrm{ox}} = \varepsilon_{\mathrm{m}} \tag{2.38}$$

However, during plastic deformation, the volume of the metal remains constant.

$$V_{\mathrm{m}} = V_{\mathrm{m}}(1+\varepsilon_{\mathrm{x,m}})(1+\varepsilon_{\mathrm{y,m}})(1+\varepsilon_{\mathrm{z,m}}) \tag{2.39}$$

The plastic deformation of the metal is supposed to be isotropic in the plane perpendicular to the tensile direction. This implies that strains in the metal along *y* and *z* directions are identical. According to Eq. 2.39, strain in the metal in the direction *y* can be written as a function of the $\varepsilon_{\mathrm{x,m}}$, the strain component in the metal in the tensile direction. The strains components are then

$$\varepsilon_{\mathrm{y,m}} = \frac{1}{\sqrt{1+\varepsilon_{\mathrm{x,m}}}} - 1 \tag{2.40}$$

According to Eq. 2.60 from Appendix, the planar stress in the oxide in the direction *i* is

$$\sigma_{\mathrm{i,ox}} = \frac{E_{\mathrm{ox}}}{1-v_{\mathrm{ox}}^2}(\varepsilon_{\mathrm{i,ox}} + v_{\mathrm{ox}}\varepsilon_{\mathrm{j,ox}}) \tag{2.41}$$

The components of the stress in the oxide due to plastic deformation of the substrate during tensile testing are

$$\sigma_{\mathrm{x,ox}} = \frac{E_{\mathrm{ox}}}{1-v_{\mathrm{ox}}^2}\left(\varepsilon_{\mathrm{x,m}} + v_{\mathrm{ox}}\left(\frac{1}{\sqrt{1+\varepsilon_{\mathrm{x,m}}}} - 1\right)\right) \tag{2.42}$$

$$\sigma_{y,ox} = \frac{E_{ox}}{1-\nu_{ox}^2}\left(\frac{1}{\sqrt{1+\varepsilon_{x,m}}} - 1 + \nu_{ox}\varepsilon_{x,m}\right) \tag{2.43}$$

The plastic deformation of the substrate remains small [35] and Taylor expansions of $(1+\varepsilon_{x,m})^{-1/2}$ in the neighbourhood of zero can be used.

$$(1+\varepsilon_{x,m})^{-1/2} = 1 - \frac{1}{2}\varepsilon_{x,m} \tag{2.44}$$

The simplified components of the stress in the oxide due to plastic deformation of the substrate during tensile testing are

$$\sigma_{x,ox} = \left(\frac{E_{ox}}{1-\nu_{ox}^2}\right)\left(1 - \frac{1}{2}\nu_{ox}\right)\varepsilon_{x,m} \tag{2.45}$$

$$\sigma_{y,ox} = \left(\frac{E_{ox}}{1-\nu_{ox}^2}\right)\left(\nu_{ox} - \frac{1}{2}\right)\varepsilon_{x,m} \tag{2.46}$$

Finally the components of the elastic strain energy during stage III of tensile testing (w_{pl}) are

$$w_{pl_{x,ox}} = \frac{1}{2}\left(\frac{E_{ox}}{1-\nu_{ox}^2}\right)\left(1 - \frac{1}{2}\nu_{ox}\right)\varepsilon_{x,m}^2 \tag{2.47}$$

$$w_{pl_{y,ox}} = -\frac{1}{2}\left(\frac{E_{ox}}{1-\nu_{ox}^2}\right)\left(\nu_{ox} - \frac{1}{2}\right)\varepsilon_{x,m}^2 \tag{2.48}$$

It is noted that the strain energy in the oxide can also be written as a function of the strain of the metal in y direction, as shown in Eqs. 2.49 and 2.50 for the situations in stages II and III respectively.

$$w_{el_{y,ox}} = \frac{1}{2}\left(\frac{E_{ox}}{1-\nu_{ox}^2}\right)\left(1 - \frac{\nu_{ox}}{\nu_m}\right)\varepsilon_{y,m}^2 \tag{2.49}$$

$$w_{pl_{y,ox}} = \frac{1}{2}\left(\frac{E_{ox}}{1-\nu_{ox}^2}\right)(1-2\nu_{ox})\varepsilon_{y,m}^2 \tag{2.50}$$

Fig. 2.14 shows evolution of stress in the oxide in x and y directions during straining. Stages I, II, III correspond to the situations from A to B, B to C and C to D respectively.

Adhesion energy (G_c) can be calculated using Eq. 2.51 where w_{ox} is the total strain energy in the oxide and h_{ox} is the oxide thickness. As in Eq. 2.52, the total strain energy is the sum of the stain energies in stages I, II and III i.e. $w_{res,ox}$, $w_{el,ox}$ and $w_{pl,ox}$ respectively. The quantified values of the adhesion energies were obtained in the range of tens to hundreds J m^{-2} for AISI 430Ti oxidised in Ar-20% O_2 at 900 ºC [31].

$$G_c = w_{ox} h_{ox} \tag{2.51}$$

$$w_{ox} = w_{res,ox} + w_{el,ox} + w_{pl,ox} \tag{2.52}$$

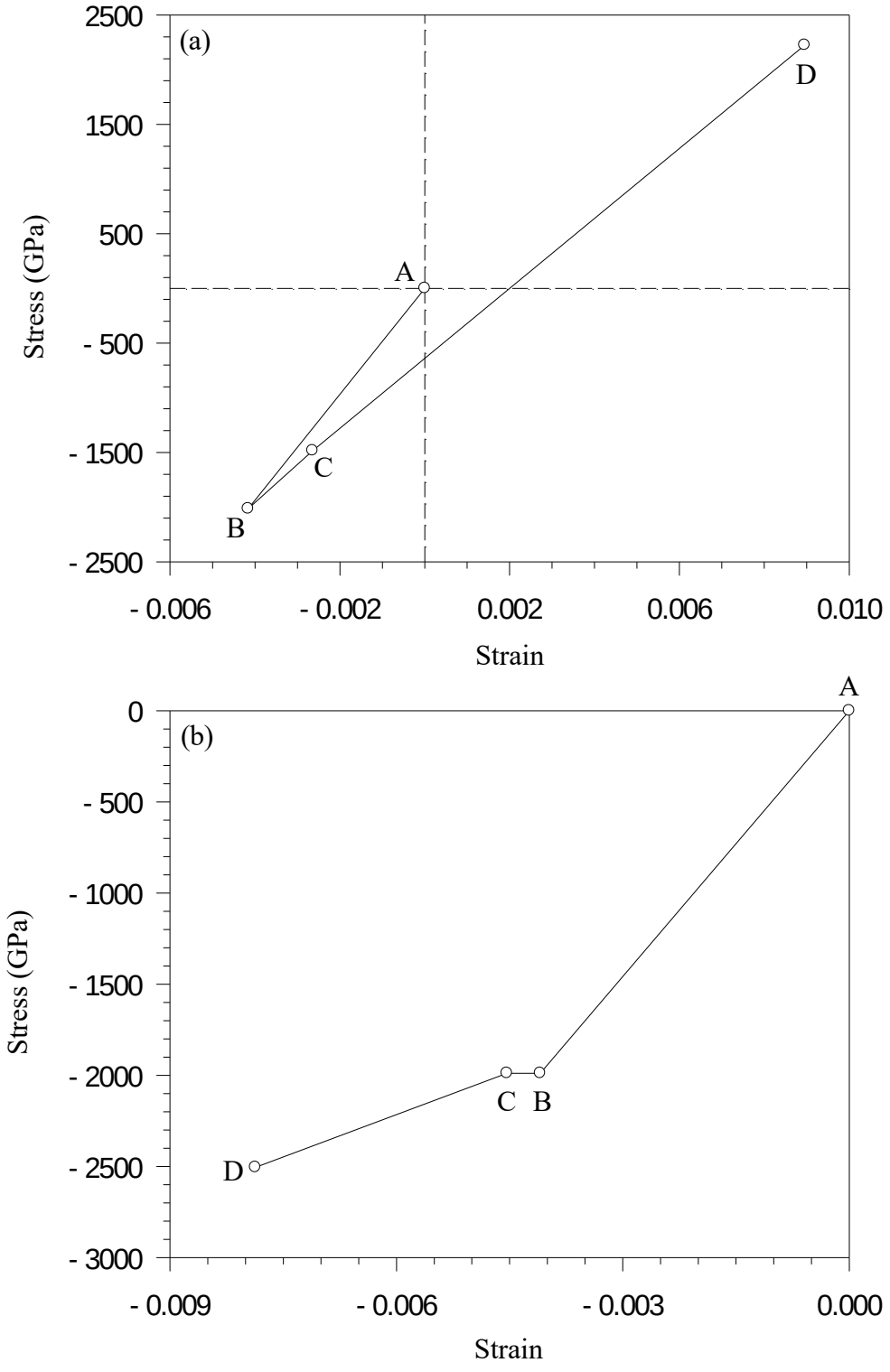

Fig. 2.14. Stress-strain curves representing the strain energies of an oxide scale thermally grown on AISI 430Ti along loading (*x*) (top) and transverse (*y*) (bottom) directions. Redrawn and adapted from S. Chandra-ambhorn et al., Mater. Sci. Technol. 23 (2007) 497–501 [31].

2.5 Summary

This chapter reviews theoretical bases and experimental methods allowing appreciating mechanical behaviour of oxide scale thermally grown on stainless steel.

Mechanical stress accumulation in oxide layer and metallic substrate is the driving force for failure. Stress originates from the coupling between the mechanical behaviour of the metal-oxide system and its chemical and microstructural changes during the oxidation process. Growth stress due to the inward diffusion of oxygen is evaluated by the Pilling-Bedworth ratio (PBR), the ratio between the molar volumes of oxide and metal. PBR values higher than one indicate the compressive stress development in the oxide while PBR values lower than one indicate the tensile stress development in the oxide which can make the oxide susceptible to fail. Growth stress can also arise from epitaxial stress, compositional changes or gradient of point defects. Stress level in the oxide cannot be directly measured and its experimental determination requires assumptions. However, considering oxide layer grown on metallic substrate as thin flat plates with a homogeneous microstructure and free from stress relieving mechanism, linear elasticity equations allow calculating the strain and the equibiaxial stress state in the plane of the oxide generated by oxide growth and thermal mismatch.

Stresses can be accommodated by elastic or plastic deformation of the oxide and/or of the metal. However, when the store energy in the oxide scale exceeds the fracture resistance of the oxide or of the metal/oxide interface, mechanical failure happens. The resulting damaging pattern depends on the stress state, the properties and the microstructure of both oxide and metal. It varies from micro-cracks to spallation. Under compression, the oxide is failed by wedging (respectively buckling) if the cohesive strength in the oxide is weaker (respectively stronger) than the metal/oxide interfacial adhesive strength. Definitions of adhesion energy (or fracture toughness) are presented through two main interrelated conditions for fracture: energy criterion and stress intensity factor. Several experiments designed to determine quantitative values of adhesion energy are also described: the inverted blister test, the modified 4-point bending test and *in-situ* tensile testing. Each configuration is characterised by loading conditions. Mode-mixed conditions of loading affect the propagation of the interfacial crack and thus the value of adhesion energy. As a consequence, comparison between values of adhesions energy obtained with different tests must be done cautiously.

Appendix: Plane Stress Analysis

This appendix summarises the hypothesis and the formulation of stress and strain in the frame of plane stress analysis.

A cubic element is submitted to stresses in every direction (Fig. 2.15). For each face of the cube:

- σ_i is the normal stress, parallel to *i* axis (*i* stands for *x*, *y* or *z*).

- $\tau_{i,j}$ and $\tau_{i,k}$ are shear stresses lying to the plane perpendicular to *i* axis. $\tau_{i,j}$ applies along the *j* direction.

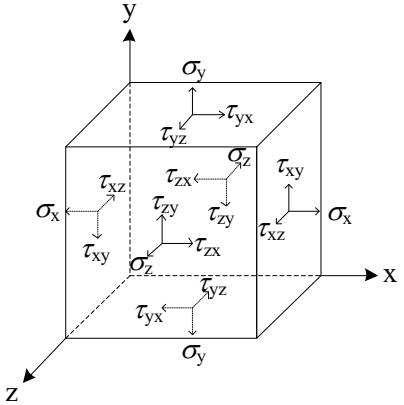

Fig. 2.15. Stress element in Cartesian coordinate.

σ_i is a normal stress applying in the direction *i* on an isotropic material. Considering a linear relation between stress and strain, Hooke's law states that the resulting strain ε_{i,σ_j} in the direction *i* is

$$\varepsilon_{i,\sigma_j} = \frac{\sigma_i}{E} \tag{2.53}$$

where *E* is the elastic or Young's modulus. The strains induced by σ_i in transverse directions *j* and *k* tend to shrink the element. It is generally assumed that ε_{j,σ_j} is linked to the normal stress via Poisson's ratio.

$$\varepsilon_{j,\sigma_j} = -v\varepsilon_{i,\sigma_j} = -v\frac{\sigma_i}{E} \tag{2.54}$$

Now considering normal stresses in every direction, the strain ε_i along the *i* direction is given by the Young's relation.

$$\varepsilon_i = \varepsilon_{i,\sigma_i} + \varepsilon_{i,\sigma_j} + \varepsilon_{i,\sigma_k} \tag{2.55}$$

Combining Eqs. 2.54 and 2.55, the strain ε_i along the *i* direction is

$$\varepsilon_i = \varepsilon_{i,\sigma_i} - v\frac{\sigma_i}{E} - v\frac{\sigma_k}{E} \tag{2.56}$$

Conversely, the expression of σ_i, the stress along the *i* direction, according to strains is given by the Lamé's relation.

$$\sigma_i = \frac{E}{(1+v)(1-2v)}\left[(1-v)\varepsilon_i + v(\varepsilon_j + \varepsilon_k)\right] \tag{2.57}$$

Oxides scales thermally grown on thick substrate can be considered as flat plates that are acted upon only by load forces that are parallel to them. In such case, the stress vector along the direction perpendicular to the film is zero. The material is said to be under plane stress.

Let consider an oxide scale in the (*x, y*) plane submitted to residual stresses and/or tensile testing. The oxide is under plane stress and σ_z is zero. In order to avoid shear stress components, τ_{zx} and τ_{zy}, the *x* axis of the frame is chosen to correspond to the tensile direction. The expression of ε_i and σ_i (*i* stands for *x* or *y*), the strain and the stress in the *i* direction, are

$$\varepsilon_i = \frac{\sigma_i}{E} - v\frac{\sigma_j}{E} \tag{2.58}$$

$$\varepsilon_z = -v\frac{\sigma_x}{E} - v\frac{\sigma_y}{E} \tag{2.59}$$

$$\sigma_i = \frac{E}{1-v^2}(\varepsilon_i + v\varepsilon_j) \tag{2.60}$$

References

[1] S.A. Bradford, Fundamentals of corrosion in gases, in: ASM International Handbook Committee (Ed.), ASM Handbook Vol. 13, ninth ed., ASM International, USA, 1987, pp. 61–76.

[2] N. Birks, G.H. Meier, F.S. Pettit, Introduction to the High Temperature Oxidation of Metals, Cambridge University Press, UK, 2006.

[3] D.J. Young, High Temperature Oxidation and Corrosion of Metals, second ed., Elsevier, The Netherlands, 2016.

[4] H.E. Evans, Stress effects in high temperature oxidation of metals, Int. Mater. Rev. 40 (1995) 1–40.

[5] P. Sarrazin, A. Galerie, J. Fouletier, Mechanisms of High Temperature Corrosion: A Kinetic Approach, Trans Tech Publications, Switzerland, 2008.

[6] R.F. Tylecote, W.K. Appleby, Some factors influencing the adherence of oxides on metals, Mater. Corros. 23 (1972) 855–859.

[7] P.Y. Hou, J. Ager, J. Mougin, A. Galerie, Limitations and advantages of Raman spectroscopy for the determination of oxidation stresses, Oxid. Met. 75 (2011) 229–245.

[8] J. Mougin, G. Lucazeau, A. Galerie, M. Dupeux, Influence of cooling rate and initial surface roughness on the residual stresses in chromia scales thermally grown on pure chromium, Mater. Sci. Eng., A 308 (2001) 118–123.

[9] S. Chandra-ambhorn, Y. Wouters, M. Dupeux, A. Galerie, L. Antoni, F. Toscan, Adhesion behaviour of thermal oxide scales grown on ferritic stainless steels proposed as interconnects in SOFCs, in: S.C. Singhal, J. Mizusaki (Eds.), Proceedings of The Electrochemical Society PV 2005–07, Canada, 2005, pp. 1816–1821.

[10] S. Chandra-ambhorn, Y. Wouters, L. Antoni, F. Toscan, A. Galerie, Adhesion of oxide scales grown on ferritic stainless steels in solid oxide fuel cells temperature and atmosphere conditions, J. Power Sources 171 (2007) 688–695.

[11] H.E. Evans, A.M. Huntz, Methods of measuring oxidation growth stresses, Mater. High Temp. 12 (1994) 111–117.

[12] A.A. Griffith, The phenomenon of rupture and flow in solids, Phil. Trans. R. Soc. Lond. A 221 (1921) 163–198.

[13] J.W. Hutchinson, Z. Suo, Mixed mode cracking in layered materials, Adv. Appl. Mech. 29 (1992) 63–191.

[14] M. Braccini, Chapter 4 Interface adherence, in: M. Braccini, M. Dupeux (Eds.), Mechanics of Solid Interfaces, John Wiley & Sons, USA, 2012, pp. 101–127.

[15] G.R. Irwin, Relation of stresses near a crack to the crack extension force, Proceedings of the Ninth Congress of Applied Mechanics, Brussels, 1956, pp. 245–251.

[16] T.L. Anderson, Fracture Mechanics: Fundamentals and Applications, third ed., CRC Press, USA, 2005.

[17] A. Galerie, F. Toscan, E. N'Dah, K. Przybylski, Y. Wouters, M. Dupeux, Measuring adhesion of Cr_2O_3 and Al_2O_3 scales on Fe-based alloys, Mater. Sci. Forum 461–464 (2004) 631–638.

[18] H. Dannenberg, Measurement of adhesion by a blister method, J. Appl. Polym. Sci. 14 (1961) 125–134.

[19] R.J. Hohlfelder, H. Luo, J.J. Vlassak, C.E.D. Chidsey, W.D. Nix, Measuring interfacial fracture toughness with the blister test. Mater. Res. Soc. Symp. Proc. 436 (1997) 115–120.

[20] M. Dupeux, A. Bosseboeuf, Application of the blister test to adhesion energy measurements in metal/ceramic film-on-substrate systems, in: A. Bellosi, T. Kosmač, A.P. Tomsia (Eds.), Interfacial Science in Ceramic Joining, Springer, The Netherlands, 1998, pp. 319–327.

[21] J. Mougin, M. Dupeux, L. Antoni, A. Galerie, Adhesion of thermal oxide scales grown on ferritic strainless steels measured using the inverted blister test, Mater. Sci. Eng., A 359 (2003) 44–51.

[22] R.J. Hohlfelder, J.J. Vlassak, W.D. Nix, H. Luo, C.E.D. Chidsey, Blister test analysis methods, Mater. Res. Soc. Symp. Proc. 356 (1995) 585–590.

[23] J. Mougin, M. Dupeux, A. Galerie, L. Antoni, Inverted blister test to measure adhesion energy of thermal oxide scales on metals or alloys, Mater. Sci. Technol. 18 (2002) 1217–1220.

[24] A. Galerie, M. Dupeux, Y. Wouters, F. Toscan, Quantitative adhesion energy values of chromia-rich thermal oxides on stainless steels determined by blister and tensile tests, Mater. Sci. Forum 522–523 (2006) 441–450.

[25] P.G. Charalambides, H.C. Cao, J. Lund, A.G. Evans, Development of a test method for measuring the mixed mode fracture resistance of bimaterial interfaces, Mech. Mater. 8 (1990) 269–283.

[26] I. Hofinger, M. Oechsner, H.-A. Bahr, M.V. Swain, Modified four-point bending specimen for determining the interface fracture energy for thin, brittle layers, Int. J. Fract. 92 (1998) 213–220.

[27] M. Zhe, O. Dezellus, G. Parry, M. Braccini, J.C. Viala, Modified 4-point bending test for adhesion measurement at the interface of iron coated with aluminum casting alloy, J. Adhes. Sci. Technol. 26 (2012) 1–17.

[28] M.M. Nagl, W.T. Evans, D.J. Hall, S.R.J. Saunders, An *in-situ* investigation of the tensile failure of oxide scales, Oxid. Met. 42 (1994) 431–449.

[29] F. Toscan, L. Antoni, Y. Wouters, M. Dupeux, A. Galerie, Oxidation kinetics and scale spallation of iron-chromium alloys with different titanium contents, Mater. Sci. Forum 461–464 (2004) 705–712.

[30] G. Bamba, Y. Wouters, A. Galerie, F. Charlot, A. Dellali, Thermal oxidation kinetics and oxide scale adhesion of Fe–15Cr alloys as a function of their silicon content, Acta Mater. 54 (2006) 3917–3922.

[31] S. Chandra-ambhorn, F. Roussel-Dherbey, F. Toscan, Y. Wouters, A. Galerie, M. Dupeux, Determination of mechanical adhesion energy of thermal oxide scales on AISI 430Ti alloy using tensile test, Mater. Sci. Technol. 23 (2007) 497–501.

[32] S. Chandra-ambhorn, P. Promdirek, G. Lothongkum, Y. Wouters, A. Galerie, Comments on the quantification of mechanical adhesion energy of thermal oxide scale on metallic substrate using tensile test, Mater. Sci. Forum 595–598 (2008) 907–914.

[33] S. Chandra-ambhorn, T. Nilsonthi, Y. Madi, A. Galerie, Application of the micro-tensile testing to investigate the adhesion of thermal oxide scales grown on AISI 441 stainless steel sheet oxidised in air and water vapour, Key Eng. Mater. 410–411 (2009) 187–193.

[34] T. Nilsonthi, S. Chandra-ambhorn, Y. Wouters, A. Galerie, Adhesion of thermal oxide scales on hot-rolled conventional and recycled steels, Oxid. Met. 79 (2013) 325–335.

[35] S. Chandra-ambhorn, N. Klubvihok, Quantification of adherence of thermal oxide scale on low carbon steel using tensile test, Oxid. Met. 85 (2016) 103–125.

[36] T. Nilsonthi, W. Issaard, S. Chandra-ambhorn, Development of the scale adhesion assessment using a tensile testing machine equipped with a CCD camera, Oxid. Met. 88 (2017) 41–55.

[37] N. Na Kalasin, S. Yenchum, T. Nilsonthi, Adhesion behaviour of scales on hot-rolled steel strips produced from continuous casting slabs, Mater. Today Proc. 5 (2018) 9359–9367.

[38] E. Fedorova, M. Braccini, V. Parry, C. Pascal, M. Mantel, F. Roussel-Dherbey, D. Oquab, Y. Wouters, D. Monceau, Comparison of damaging behavior of oxide scales grown on austenitic stainless steels using tensile test and cyclic thermogravimetry, Corros. Sci. 103 (2016) 145–156.